BASIC ADVANCES IN THE FINITE-VOLUME METHOD FOR TRANSONIC POTENTIAL FLOW CALCULATIONS

D. A. Caughey* and Antony Jameson**
Cornell University Princeton University
Ithaca, New York 14853 Princeton, New Jersey 08540

ABSTRACT

The finite-volume method of Jameson and Caughey provides a framework within which it is possible to calculate transonic potential flows about essentially arbitrary geometrical configurations. Improvements designed to increase the accuracy of the basic scheme and its consistency in the far field will be described. These include the incorporation of an artificial viscosity which maintains the formal second-order accuracy of the scheme in supersonic zones, and a modification of the flux balances to allow the free-stream conditions to satisfy the difference equations identically. Results of calculations illustrating the importance of these effects will be presented.

I. Introduction

The finite-volume methods of Jameson and Caughey[1,2,3] provide a general framework within which it is relatively easy to calculate the transonic potential flow past essentially arbitrary geometrical configurations. Like finite-element methods, these methods use only local properties of the transformations which generate the difference-grid. This feature essentially decouples the solution of the transonic flow equations from the grid-generating step, so that minor modifications of a universal algorithm can be applied in any boundary-conforming coordinate system. Although the initial variants of these methods used line relaxation to solve the difference equations, the multi-grid/alternating-direction-implicit (MAD) scheme of Jameson[4] has also been applied to provide high rates of convergence to very small residuals for two-dimensional calculations.[5]

Two particular features of the formulation of the finite-volume methods will be addressed in the present paper, with the aim of improving the accuracy and consistency of the method. The first is an improved artificial viscosity which allows retention of formal second-order accuracy in supersonic zones; the second is a modification of the scheme which allows the freestream conditions to be satisfied identically by the difference equations. In the following sections, the fully-conservative finite-volume method will first be briefly reviewed, including the changes necessary to retain second-order accuracy in supersonic zones. The problem of consistency with the free-stream solution will then be discussed and a remedy proposed. Finally, results of calculations incorporating these changes will be presented and discussed.

II. Analysis

A. Finite-Volume Scheme

For convenience, here and throughout the paper the analysis will be described for a two-dimensional problem, and only distinguishing features of the extension to three-dimensional problems will be discussed. The equations of steady, inviscid, isentropic flow can be represented as follows. Let x,y be Cartesian coordinates and u,v be the corresponding components of the velocity vector q. Then the continuity equation can be written as

$$(\rho u)_x + (\rho v)_y = 0, \tag{1}$$

where ρ is the local density. This is given by the isentropic law

$$\rho = (1 + \frac{k-1}{2} M_\infty^2 (1 - q^2))^{\frac{1}{k-1}} \tag{2}$$

where k is the ratio of specific heats, and M_∞ is the freestream Mach number. The pressure p and the speed of sound a follow from the relations

$$p = \rho^k / (k M_\infty^2), \tag{3}$$

and

$$a^2 = \rho^{k-1} / M_\infty^2. \tag{4}$$

---

*Associate Professor, Sibley School of Mechanical and Aerospace Engineering.

**Professor, Department of Mechanical and Aerospace Sciences.

Consider now a transformation to a new set of coordinates X,Y. Let the Jacobian matrix of the transformation be defined by

$$H = \begin{Bmatrix} x_X & x_Y \\ y_X & y_Y \end{Bmatrix}, \tag{5}$$

and let h denote the determinant of H. The metric tensor of the new coordinate system is given by the matrix H^TH, and the contravariant components of the velocity vector U,V are given by

$$\begin{Bmatrix} U \\ V \end{Bmatrix} = H^{-1} \begin{Bmatrix} u \\ v \end{Bmatrix} = (H^TH)^{-1} \begin{Bmatrix} \phi_X \\ \phi_Y \end{Bmatrix} \tag{6}$$

where ϕ is the velocity potential. Eq.(1), upon multiplication by h, can then be written

$$(\rho hU)_X + (\rho hV)_Y = 0. \tag{7}$$

The fully-conservative finite-volume approximation corresponding to Eq.(7) is constructed by assuming separate bilinear variations of the independent and dependent variables within each mesh cell.

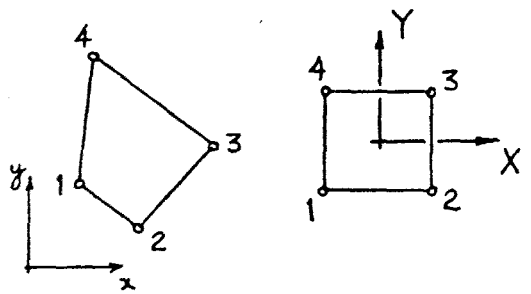

Mesh cell in Physical and Computational Domains.

Numbering the cell vertices as illustrated in the sketch above, and assuming that the local coordinates $X_i = \pm 1/2$, $Y_i = \pm 1/2$ at the vertices, the local mapping can be written

$$x = 4\sum_{i=1}^{4} x_i(1/4 + X_iX)(1/4 + Y_iY), \tag{8}$$

where x_i is the x-coordinate of the i-th vertex. Similar formulas are assumed to hold for y and ϕ. At a cell center, this transformation yields formulas for derivatives such as

$$x_X = 1/2(x_2 - x_1 + x_3 - x_4). \tag{9}$$

If we introduce the averaging and differencing operators

$$\begin{aligned} \mu_X f_{i,j} &= 1/2(f_{i+1/2,j} + f_{i-1/2,j}), \\ \delta_X f_{i,j} &= (f_{i+1/2,j} - f_{i-1/2,j}), \end{aligned} \tag{10}$$

then the transformation dervivatives, evaluated at the cell centers, can be expressed by formulas such as

$$\begin{aligned} x_X &= \mu_Y \delta_X x \\ x_Y &= \mu_X \delta_Y x \end{aligned} \tag{11}$$

with similar expressions for the derivatives of y and the potential. Such formulas can be used to determine ρ, h, U, and V at the center of each cell using Eqs.(2),(5), and (6). Eq.(7) is represented by conserving fluxes across the boundaries of auxiliary cells whose faces are chosen to be midway between the faces of the primary mesh cells. This can be represented as

$$\mu_Y \delta_X(\rho hU) + \mu_X \delta_Y(\rho hV) = 0. \tag{12}$$

This formula can also be obtained by applying the Bateman variational principle that the integral of the pressure

$$I = \int p \, dx \, dy \tag{13}$$

is stationary, and approximating I by a simple one-point integration scheme in which the pressure at the center of each grid cell is multiplied by the cell area. For subsonic flow the finite-volume method can equally well be regarded as a finite element method with isoparametric bi-linear elements.

The extension to treat transonic flows is accomplished by adding an artificial viscosity to introduce an upwind bias. The use of the one-point integration scheme leading to Eq.(12) has the advantage of requiring only one density evaluation per mesh point, but also has the undesirable effect of tending to decouple the solution at odd- and even-numbered points of the grid, and suitable recoupling terms can be added to improve the stability of the solution. If we represent the influence coefficients of the terms containing ϕ_{XX} and ϕ_{YY} in the expanded form of Eq.(12) as

$$\begin{aligned} A_X &= \rho h(g^{11} - U^2/a^2) \\ A_Y &= \rho h(g^{22} - V^2/a^2) \end{aligned} \tag{14}$$

where g^{ij} are the elements of $(H^TH)^{-1}$, then the compensated equation can be written

$$\begin{aligned} \delta_X \mu_Y(\rho hU) + \delta_Y \mu_X(\rho hV) - \\ \frac{\varepsilon}{2} \delta_{XY}(A_X + A_Y) \delta_{XY} \phi = 0, \end{aligned} \tag{15}$$

where $0 \le \varepsilon \le 1/2$. In practice $\varepsilon = 1/2$ is generally used. An alternative method of obtaining the recoupling terms is to use a higher-order integration scheme which takes account not only of the pressure at the center of each cell, but also its x- and y- derivatives.

Second-order Viscosity

The original scheme was stabilized in supersonic regions by the explicit addition of an artificial viscosity, chosen to emulate the directional bias introduced by the rotated difference scheme of Jameson.[6] We defined

$$\begin{aligned}\hat{P} &= \rho h\sigma/a^2(U^2\,\delta_{XX} + UV\,\delta_{XY})\phi \\ \hat{Q} &= \rho h\sigma/a^2(UV\,\delta_{XY} + V^2\,\delta_{YY})\phi,\end{aligned} \tag{16}$$

where the switching function

$$\sigma = \max(0.,\ 1 - (M_c/M)^2) \tag{17}$$

is non-zero only for values of the local Mach number $M = q/a$ greater than some critical Mach number M_c. Then, after defining

$$P_{i+1/2,j} = \begin{cases} \hat{P}_{i,j} & \text{if } U \geq 0, \\ -\hat{P}_{i+1,j} & \text{if } U < 0, \end{cases} \tag{18}$$

with a similar shift for Q, we represented Eq.(15) as

$$\begin{aligned}&\delta_X(\mu_Y(\rho hU) + P) + \delta_Y(\mu_X(\rho hV) + Q) \\ &\quad - \tfrac{\varepsilon}{2}\,\delta_{XY}(A_X + A_Y)\,\delta_{XY}\phi = 0.\end{aligned} \tag{19}$$

The difference Eqs.(15) approximate the original differential Eq.(7) to within a formal truncation error of second order in the mesh spacing in the physical plane when the mesh is smooth. Since the additional fluxes P and Q added in supercritical regions are of order of the physical mesh spacing, however, Eqs.(19) approximate Eq.(7) to within a truncation error of only first order in the mesh spacing. The error resulting from the introduction of the artificial viscosity can be reduced to second order at nearly all points in the flowfield if we define

$$P_{i+1/2,j} = \begin{cases} \hat{P}_{i,j} - (1 - \varkappa\delta_X\rho)\hat{P}_{i-1,j} & \text{if } U \geq 0, \\ -\hat{P}_{i+1,j} + (1 - \varkappa\delta_X\rho)\hat{P}_{i+2,j} & \text{if } U \leq 0, \end{cases} \tag{20}$$

where $\varkappa$ is a constant of order unity. In regions where the solution is smooth, the term $\varkappa\delta_X\rho$ is of first order in the mesh spacing, and the viscosity is formally a second order quantity. Near a shock, the quantity $(1 - \varkappa\delta_X\rho)$ becomes small, and Eqs.(20) approximate Eqs.(18) — i.e., the viscosity reverts to a first-order quantity. This hybridization of the second-order scheme has been found necessary to stabilize computations for solutions containing strong shocks.

Freestream Consistency

The implementation of the algorithm is simplified by introducing the reduced potential G describing perturbations from a uniform free stream, inclined at an angle α to the x-axis

$$G = \phi - x\cos\alpha - y\sin\alpha. \tag{21}$$

The contravariant velocities are then calculated in two steps, first determining

$$\begin{Bmatrix} u \\ v \end{Bmatrix} = H^{T^{-1}} \begin{Bmatrix} G_X \\ G_Y \end{Bmatrix} + \begin{Bmatrix} \cos\alpha \\ \sin\alpha \end{Bmatrix}, \tag{22}$$

then using the first of Eqs.(6) to determine U and V. For two-dimensional problems, this procedure has the attractive feature that the freestream conditions (i.e., $G = 0$) identically satisfy the difference equations. This is easily verified since at each cell center in this case

$$h\begin{Bmatrix} U \\ V \end{Bmatrix} = \begin{Bmatrix} \mu_X\delta_Y\, y\cos\alpha - \mu_X\delta_Y\, x\sin\alpha \\ -\mu_Y\delta_X\, y\cos\alpha + \mu_Y\delta_X\, x\sin\alpha \end{Bmatrix}. \tag{23}$$

The density is calculated using the Cartesian velocities from Eqs.(22) in Eq.(2). For the freestream condition, this gives $\rho = 1$ and Eq.(12) becomes

$$\begin{aligned}&\mu_Y\delta_X(\mu_X\delta_Y\, y\cos\alpha - \mu_X\delta_Y\, x\sin\alpha) \\ &\quad + \mu_X\delta_Y(-\mu_Y\delta_X\, y\cos\alpha + \mu_Y\delta_X\, x\sin\alpha) = 0,\end{aligned} \tag{24}$$

since the averaging and differencing operators commute.

In three-dimensional problems, the difference equations do not admit $G = 0$ as a solution because the elements of H^{-1} consist of nonlinear products of the mapping derivatives, and the averaging and differencing operators do not cancel identically. For example, the x-component of the free stream is given by

$$h\begin{Bmatrix} U \\ V \\ W \end{Bmatrix} = \begin{Bmatrix} y_Y z_Z - y_Z z_Y \\ y_Z z_X - y_X z_Z \\ y_X z_Y - y_Y z_X \end{Bmatrix} \cos\alpha. \tag{25}$$

At the cell centers, the fluxes are represented by

$$h\begin{Bmatrix} \bar{U} \\ \bar{V} \\ \bar{W} \end{Bmatrix} = \begin{Bmatrix} \mu_{XZ}\delta_Y y\,\mu_{XY}\delta_Z z - \mu_{XY}\delta_Z y\,\mu_{XZ}\delta_Y z \\ \mu_{XY}\delta_Z y\,\mu_{YZ}\delta_X z - \mu_{YZ}\delta_X y\,\mu_{XY}\delta_Z z \\ \mu_{YZ}\delta_X y\,\mu_{XZ}\delta_Y z - \mu_{XZ}\delta_Y y\,\mu_{YZ}\delta_X z \end{Bmatrix} \cos\alpha, \tag{26}$$

and the (three-dimensional equivalent of) Eq.(12) becomes

$$\mu_{YZ}\delta_X(h\bar{U}) + \mu_{XZ}\delta_Y(h\bar{V}) + \mu_{XY}\delta_Z(h\bar{W}) = R, \quad (27)$$

which is not identically zero for an arbitrary smooth mesh. It can be verified, in fact, that Eq.(27) results in

$$R = 1/2(\mu_X\delta_X((\mu_Y\delta_Y y)(\mu_Z\delta_Z z)-(\mu_Z\delta_Z y)(\mu_Y\delta_Y z)) + \mu_Y\delta_Y((\mu_Z\delta_Z y)(\mu_X\delta_X z)-(\mu_X\delta_X y)(\mu_Z\delta_Z z)) + \mu_Z\delta_Z((\mu_X\delta_X y)(\mu_Y\delta_Y z)-(\mu_Y\delta_Y y)(\mu_X\delta_X z)))\cos\alpha \ . \quad \ldots \quad (28)$$

If the Cartesian coordinates are expanded in Taylor series about their values at the central point shared by the eight neighboring mesh cells contributing to the residual in Eq.(28), the residual can be verified to be a fourth-order quantity in the local mesh spacing. Since in our formulation the residuals of Eq.(12) are of second order in the mesh spacing, this effect corresponds to a second-order error in the residual. This is consistent with the overall second-order accuracy of the scheme in subsonic regions, but since the mesh cells are necessarily quite large far from the body in three-dimensional calculations, it was thought that the error introduced by this discretization of the free-stream contribution might be important.

In order to assess the significance of this error, calculations were performed with this source of error removed from the residual by re-writing Eq.(12) as

$$\mu_{YZ}\delta_X(\rho hU - h\bar{U}) + \mu_{XZ}\delta_Y(\rho hV - h\bar{V}) + \mu_{XY}\delta_Z(\rho hW - h\bar{W}) = 0, \quad (29)$$

where $h\bar{U}$, $h\bar{V}$, $h\bar{W}$ were calculated using formulas similar to Eqs.(26), but which also included the y-component of the free-stream velocity. Since these formulas can be considered approximations to Eqs.(25), it is easily verified that the added terms do cancel identically when evaluated analytically. When evaluated numerically, however, they cancel exactly the error introduced by the contribution of the free stream to the total fluxes. At boundary points it is necessary to devise reflection rules for these artificial fluxes. Our procedure was to continue the fluxes in the plane parallel to the boundary across the boundary unchanged; the flux normal to the boundary was corrected by retaining the first term in a Taylor series expansion of the component of Eq.(25) normal to the boundary, evaluating all differences at the centers of the cells immediately adjacent to the boundary. This scheme, when applied to the two-dimesional form of the difference equations maintains its self-cancelling property; in the three-dimensional case, it has the effect of replacing the differences in Eq.(28) taken normal to the boundary by one-sided formulas.

B. Boundary Conditions and Grid Generation

An important advantage of the finite-volume method is its decoupling of the solution procedure from the grid-generation step. This permits the grid to be generated in any convenient manner, and allows application of an essentially universal algorithm to any problem for which a boundary-conforming coordinate system can be generated.

The airfoil calculations to be described were computed on a mesh generated by weakly shearing the conformal mapping to a circle of the Joukowsky airfoil most closely approximating the actual airfoil in the leading-edge region. Details of this coordinate system are contained in Reference 5. The three-dimensional calculations were computed on a mesh generated by the Cylindrical/Wind-tunnel mapping sequence described in References 2 and 3.

Two types of boundary conditions must be specified to determine solutions for the potential flow problems considered herein. The no-flux condition must be enforced across any solid boundaries (such as the airfoil, wing and fuselage surfaces); and appropriate far-field boundary conditions must be specified at the necessarily finite limits of the computational domain. In addition, for the airfoil calculations, a discontinuity in potential across some branch cut must be incorporated if the airfoil has lift. For the three-dimensional calculations, a linearized treatment of the vortex sheet is used. It assumes that constant strength vortex filaments trail downstream of the wing trailing edge in the nearly streamwise computational surfaces. The values of reduced potential on the sheet are determined by requiring the velocity normal to the assumed location of the sheet to be continuous across the sheet.

The solid-surface boundary conditons are quite easy to enforce in boundary-conforming coordinate systems because the difference scheme is formulated in terms of the contravariant components of the velocity. The appropriate condition is that the out-of-plane component be zero. This is incorporated by reflection of the normal-flux contributions for the cells immediately adjacent to the boundary.

A disadvantage of the finite-volume schemes is the need to truncate the usually infinite domains of aerodynamic interest to finite computational regions. This is in contrast to methods in which the equation can be analytically transformed with suitable stretching functions so that the difference mesh extends to infinity. (See, e.g., References 6, 7, and 8.) In the analyses treated here, a reduced potential is introduced to describe the perturbations upon an otherwise uniform stream. This potential is set to values appropriate for a compressible vortex of circulation Γ,

$$\phi = \frac{\Gamma}{2\pi} \arctan \left(y\sqrt{1 - M_\infty^2}/x \right) \qquad (30)$$

on the farfield boundaries of the computational domain for the airfoil calculations. The reduced potential is set to zero on the upstream and lateral farfield boundaries for the three-dimensional calculations; the first derivative in the streamwise direction of the reduced potential is set to zero on the downstream boundary. This is consistent with the assumption that the flow properties have become invariant in the streamwise direction. If the freestream is in the x direction, irrotationality then implies that $\partial u/\partial y = \partial v/\partial x = 0$ and $\partial u/\partial z = \partial w/\partial x = 0$, and consequently that the streamwise velocity component has its free-stream value.

C. Solution of Difference Equations

The difference equations resulting from this formulation are solved iteratively. A relatively conventional successive-line-overrelaxation (SLOR) scheme is used in the computer codes which solve the three-dimensional problems, with care taken in the formulation of the algorithm to model the correct domains of dependence. The solutions to be presented were coaculated on a sequence of three grids, each containing eight times the number of mesh cells of the preceeding one. On each of the coarser grids, 200 relaxation sweeps were performed, and the solution was used as an initial estimate for the solution on the next grid. Only 100 iterations were performed on the finest grid. This is sufficient to remove nearly all of the high wave-number error, but the lift may not be completely converged. Since we will only compare results obtained in a similar manner, however, this lack of convergence should not introduce a serious systematic error. Details of the relaxation scheme can be found in Reference 1 and 2. The two-dimensional results to be presented were calculated using a fine-volume generalization of Jameson's Multi-grid/ Alternating-direction (MAD) algorithm.[4,5]

III. Results

Results will now be presented to demonstrate the effects of the improved accuracy of the second-order viscosity and the removal of the truncation error of the free stream. The results for the improved viscosity will be presented for two-dimensional calculations; the results with the free stream contribution to the residuals subtracted out will necessarily be presented for a three-dimensional geometry.

Figures 1(a) and 1(b) show the surface pressure distributions calculated for the flow at a free-stream Mach number of 0.75 past an NACA 0012 airfoil at 2 degrees angle of attack. Both results were calculated using the same grid, consisting of 128x32 mesh cells in the circumferential and radial directions, respectively. Figure 1(a) shows the result using the first-order accurate viscosity; Figure 1(b) shows the result using the second-order formulation. The result using the first-order viscosity clearly underpredicts the size of the supersonic pocket above the airfoil and, consequently, underpredicts the lift. That the second-order accurate result is, in fact, nearer the exact answer is verified by the convergence study plotted in Figure 2 for this case, calculated using sequences of grids for each scheme. The calculated lift and drag coefficients are plotted against mesh spacing for the first-order scheme, while the results of the second-order scheme are plotted against the square of the mesh spacing. (NX is the number of mesh cells in the circumferential direction.) Both schemes clearly converge in the limit of zero mesh spacing to the same lift and drag coefficients, but on the 128x32 grid, the error in lift coefficient calculated using the first-order scheme is still almost 10 per cent. For the second-order scheme the error is less than 3 percent.

Results of the first- and second-order schemes for a shockfree solution are shown in Figures 3(a) and 3(b). The surface pressure distributions are plotted for the Korn airfoil (Catalog No. 75-06-12)[9] at a free-stream Mach number of 0.75 and zero angle of attack. These conditions correspond to the shockfree design point for this airfoil, so the exact solution should have a smooth recompression back through the sonic velocity at the downstream boundary of the supersonic pocket above the airfoil. Results are shown for the first-order scheme in Figure 3(a) and for the second-order scheme in Figure 3(b). Both solutions were obtained on identical grids containing 128x32 mesh cells. The second-order-accurate scheme produces an almost shock-free result, whose pressure distribution is much nearer the hodograph solution. The calculated drag coefficient still differs appreciably from zero, but the solution calculated on a 256x64 mesh results in a drag coefficient of only .0005.

The three-dimensional calculations were performed for the ONERA wing M-6, mid-mounted on a circular cylinder. The wing geometry is described in Reference 10, and other calculations for this wing-cylinder combination are presented in References 1-3. A perspective view of the wing-fuselage grid (corresponding to the coarsest of the three grids used) is pictured in Figure 4. Calculations were performed on an identical grid containing 160x24x32 mesh cells using the basic algorithm of References 1 and 3 and the

modification described herein to remove the free-stream contribution to the residual. The wing lift coefficients were 0.3106 and 0.3120 for the original and modified schemes, respectively. The discrepancy in lift coefficient was therefore less than one-half of one per cent. At inboard stations, the wing surface pressure distributions are virtually indistinguishable. The streamwise surface pressure coefficients are compared at two outboard span stations in Figures 5(a) and 5(b). As can be seen, even here the details of the pressure distributions are in excellent agreement, including at the 72 percent semi-span station where the leading and trailing-edge shocks are beginning to merge. The excellent agreement between the two sets of results indicates that the truncation error introduced by the inconsistency between the free-stream conditions and the difference equations introduces no serious error, at least in the vicinity of the body. A similar inconsistency in a finite-volume scheme for the Euler equations developed by Pulliam and Steger[11] has also been reported to cause no serious error. In view of the additional labor involved in calculating the free-stream fluxes, particularly at the boundaries in the present scheme, the original scheme is probably to be preferred.

IV. Conclusions

Several fundamental improvements to the finite-volume method for the calculation of transonic potential flows have been presented. The incorporation of an improved artificial viscosity which retains the second-order accuracy of the basic scheme except in the immediate vicinity of shocks is shown to be necessary for the proper prediciton of lift when calculations are performed on reasonably coarse meshes. The lack of consistency of the difference equations with a uniform free stream is shown, by comparison with a modified scheme which subtracts this contribution, to produce small errors.

V. Acknowledgements

This work was supported in part by the Office of Naval Research under Contracts N00014-77-C-0032 and N00014-77-C-0033, and by NASA under Grants NSG-1579 and NGR-33-016-201. It is a particular pleasure on this occasion to thank Morton Cooper for his continued interest in and support of this work.

VI. References

1. Jameson, Antony and Caughey, D.A., "A Finite-Volume Method for Transonic Potential Flow Calculations," Proc. of AIAA 3rd Computational Fluid Dynamics Conference, pp. 35-54, Albuquerque, N.M., June 27-29, 1977.

2. Caughey, D.A. and Jameson, Antony, "Numerical Calculation of Transonic Potential Flow about Wing-Body Combinations," AIAA Journal Vol. 17, pp. 175-181, February 1979.

3. Caughey, D.A. and Jameson, Antony, "Progress in Finite-Volume Calculations for Wing-Fuselage Combinations," AIAA Journal Vol. 18, pp. 1281-1288, November 1980.

4. Jameson, Antony, "A Multi-Grid Scheme for Transonic Potential Calculations on Arbitrary Grids," Proc. of AIAA 4th Computational Fluid Dynamics Conference, pp 122-146, Williamsburg, Va., July 23-25, 1979.

5. Jameson, Antony, Caughey, D. A., Steinhoff, John, Jou, W. H., and Pelz, Richard, "Accelerated Finite-Volume Calculation of Transonic Potential Flows," Proc. of GAMM Specialist Workshop for Numerical Methods in Fluid Dynamics, Stockholm, September 1979.

6. Jameson, Antony, "Iterative Solution of Transonic Flows over Airfoils and Wings including Flows at Mach 1," Comm. Pure and Appl. Math. Vol 27, pp. 283-309, 1974.

7. Jameson, Antony and Caughey, D.A., "Numerical Calculation of the Transonic Flow past a Swept Wing," New York University ERDA Report COO-3077-140, June 1977.

8. Caughey, D.A. and Jameson, Antony, "Accelerated Iterative Calculation of Transonic Nacelle Flowfields," AIAA Journal Vol. 15, pp.1474-1480, October 1977.

9. Bauer, Frances, Garabedian, Paul, Korn, David, and Jameson, Antony, Supercritical Wing Sections II, Springer-Verlag, New York, 1975.

10. Monnerie, B., and Charpin, F., "Essais de Buffeting d'une Aile en Fleche en Transsonique," 10e Colloque d'Aerodynamique Applique, Lille, France, November 1973.

11. Pulliam, T. H., and Steger, J. L., "Implicit Finite-Difference Simulations of Three-dimensional Compressible Flow," AIAA Journal Vol. 18, pp. 159-167, February 1980.

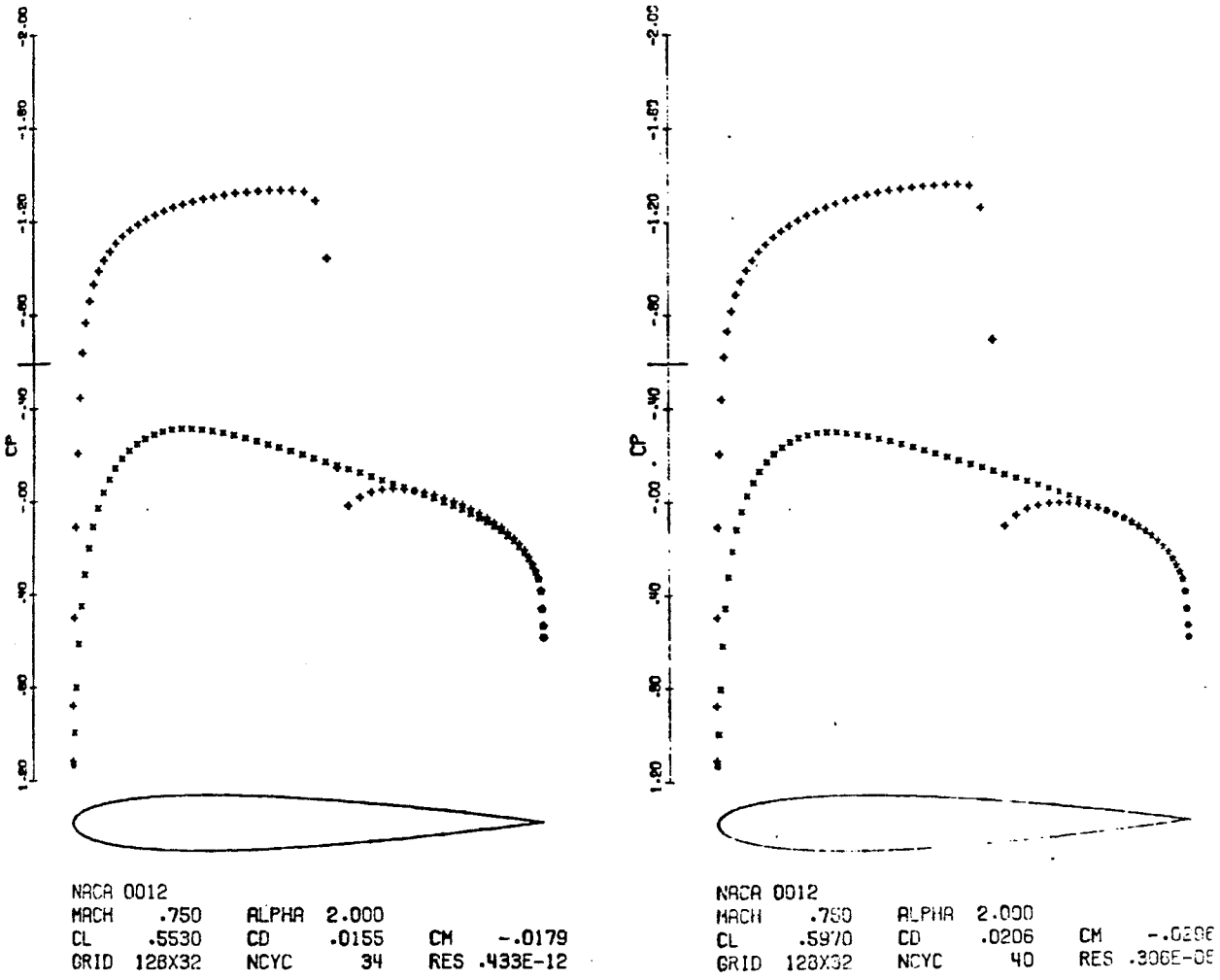

(a) First-order scheme

(b) Second-order scheme

Figure 1. Surface pressure distributions for transonic flow past NACA 0012 airfoil at 0.75 Mach number and 2 degrees angle of attack.

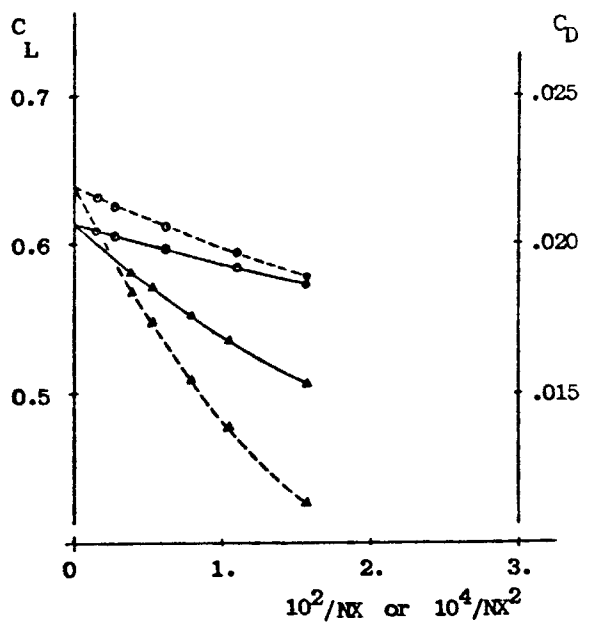

Figure 2. Convergence of lift and drag coefficients with mesh spacing for first- and second-order schemes. NACA 0012 at 0.75 Mach number and 2 degrees angle of attack. Triangles represent first-order scheme; circles represent second-order scheme. Solid line connects results for lift coefficient; dashed line connects results for drag coefficient.

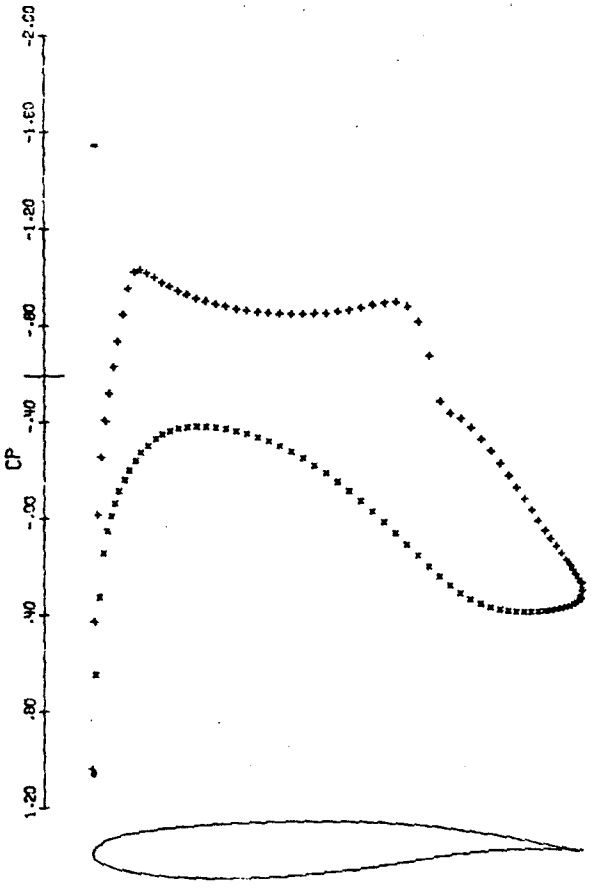

(a) First-order scheme

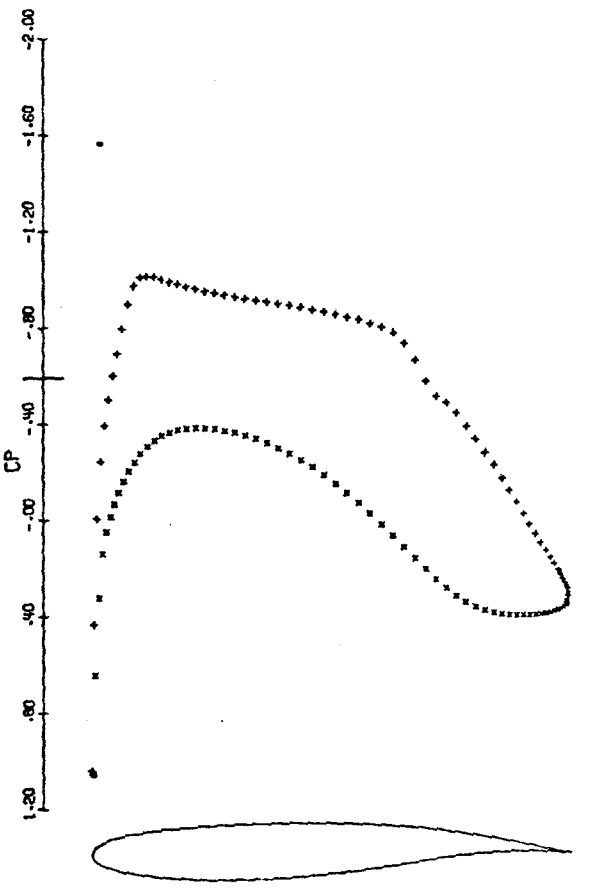

(b) Second-order scheme

Figure 3. Surface pressure distributions for transonic flow past Korn airfoil at shock-free design point.

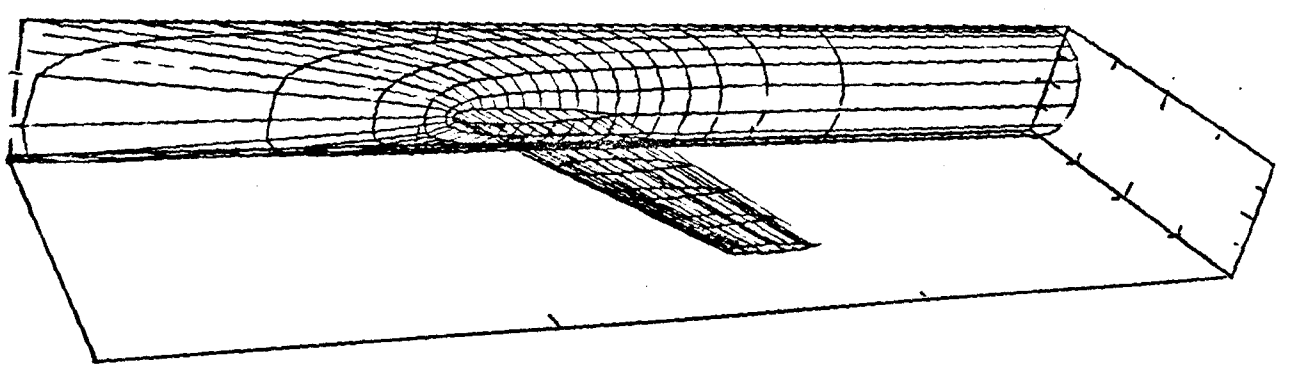

Figure 4. Wing and fuselage grid system for ONERA Wing/Cylinder configuration.

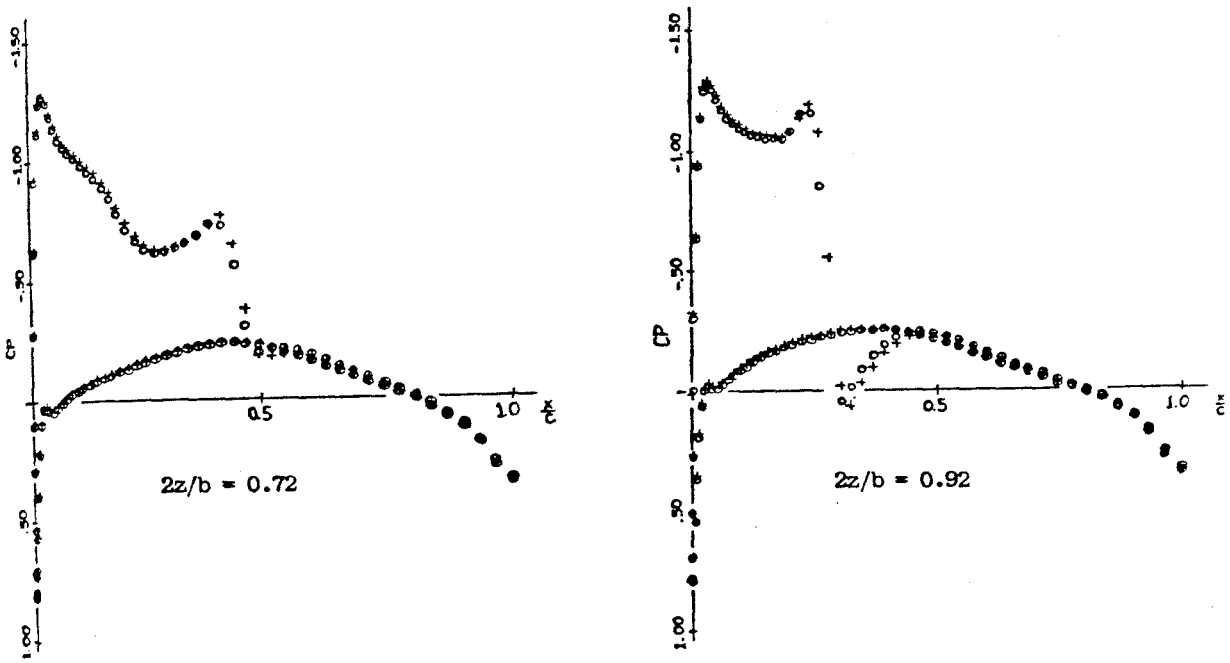

(a) 72 per cent semi-span

(b) 92 per cent semi-span

Figure 5. Streamwise wing surface pressure distributions for ONERA Wing/Cylinder Combination. Circles represent original scheme; crosses represent modified scheme with free-stream fluxes removed from residuals.